Fabrication of Fe-bismuth Borate Glasses and their Efficient Radiation Shielding Performance Using XCOM, MCNP5, and Phy-X/PSD Program

S. E. Shaban[a*], M. A. Samei[a], E. M. Abou Hussein[b]

[a]*Safeguards and Physical Protection Dep., Nuclear and Radiological Safety Research Center, Egyptian Atomic Energy Authority, Cairo, Egypt*

[b]*Radiation Chemistry Dep., National Centre for Radiation Research and Technology, Egyptian Atomic Energy Authority, Cairo, Egypt*

smh_elsaid@yahoo.com

Keywords: *Bismuth borate glass, HPGe detector, Gamma-ray attenuation, MAC, ESR*

Fe-doped bismuth borate glass systems containing 0.0, 0.5, 1.0, and 1.5 mol% Fe_2O_3 were synthesized via the melt–quench technique, with measured densities increasing from 2.889 to 2.952 g/cm³ as Fe_2O_3 content increased. The gamma-ray attenuation performance of the prepared glasses was experimentally evaluated using a high-purity germanium (HPGe) detector at photon energies of 0.662, 1.173, and 1.333 MeV, and theoretically assessed over a wide energy range (0.015–15 MeV) using XCOM, MCNP5, and Phy-X/PSD programs. The experimental mass attenuation coefficients (MAC) showed excellent agreement with theoretical predictions, with deviations within acceptable statistical limits. The results reveal strong energy dependence of attenuation parameters, with high MAC and Linear Attenuation Coefficient (LAC) values at low photon energies dominated by photoelectric absorption, followed by gradual reduction in the Compton scattering region and near-constant behavior at high energies where pair production prevails. Fe_2O_3 doping slightly modifies low-energy attenuation behavior and effective atomic number without compromising shielding efficiency at medium and high energies. Half Value Layer (HVL) and Mean Free Path (MFP) analyses further confirm the superior attenuation capability of the investigated glasses, particularly at low energies. Electron spin resonance (ESR) analysis revealed no detectable changes in g-value, linewidth, or signal intensity after gamma irradiation up to 60 kGy, indicating high structural stability and strong resistance to radiation-induced defects. These findings demonstrate that Fe-doped bismuth borate glasses are structurally stable, lead-free, and compositionally tunable materials with a potential for radiation-shielding applications in nuclear, medical, and industrial environments.

Introduction

Glasses have gained considerable attention as alternative materials for radiation shielding, owing to their favorable physical, chemical, and optical properties [1]. Compared to traditional shielding materials such as concrete, rock, mud, and polymers, glass offers advantages including structural homogeneity, transparency, ease of fabrication, and tunable composition. Among various heavy-metal-oxide

systems, bismuth-containing glasses have emerged as particularly promising due to the high atomic number and large photoelectric cross section of Bi^{3+} ions, which markedly enhance photon attenuation without introducing the toxicity and environmental hazards associated with lead-based systems [2-7].

For a comprehensive evaluation of shielding performance, the mass attenuation coefficient (μ/ρ) remains one of the most fundamental parameters, as it directly reflects the probability of photon interaction within the material. Accurate (μ/ρ) values can be obtained experimentally or predicted using established theoretical tools, including XCOM, MCNP5, and the Phy-X/PSD platform, each providing robust photon–matter interaction data across a wide energy range [8-12].

When integrated with experimental validation using high-resolution detectors such as HPGe systems, these approaches enable precise characterization of gamma-ray attenuation behavior and facilitate calculation of additional shielding indicators such as LAC, HVL, MFP, and effective atomic number (Z_eff) [12-15]. These parameters provide a comprehensive understanding of a material's shielding efficiency [16-19].

Extensive literature reports the use of borate, silicate, phosphate, tellurite, and heavy-metal-rich glass systems for radiation shielding applications [20]. However, despite significant progress, the combined influence of Fe_2O_3 doping and bismuth-rich borate networks remains insufficiently explored, particularly regarding the interplay between structural modifications, defect stability, and shielding efficiency. Iron is a technologically important dopant due to its ability to exist in multiple oxidation states (Fe^{2+}/Fe^{3+}), participate in redox equilibria, and alter the glass network connectivity. These features not only affect the physical and optical properties but may also influence the material's behavior under high irradiation doses.

Addressing these gaps, the present study provides a comprehensive experimental and theoretical investigation of Fe-doped bismuth borate glasses by correlating gamma-ray attenuation parameters with detailed structural analysis before and after gamma irradiation. The XCOM, MCNP5, and Phy-X/PSD were used to calculate shielding parameters, including (μ/ρ) values, HVL, MFP, and LAC for all samples [21–28].

By integrating HPGe-based measurements with XCOM, MCNP5, and Phy-X/PSD simulations, and by examining radiation-induced structural changes through electron spin resonance (ESR), this work establishes a direct link between Fe_2O_3 concentration, glass network stability, and shielding performance. This systematic approach not only clarifies the role of Fe in enhancing attenuation behavior but also highlights the potential of these glasses as a lead-free radiation shielding materials suitable for some technological applications in laboratories and facilities that deal with the hazards of ionizing radiation, like dentistry,

healthcare, aerospace, and industrial environments [29-32].

Experimental

Glass preparation

Four bismuth borate glass samples, denoted F1–F4, were prepared by the melting-quenching technique using high-purity materials and a well-established melting-annealing procedure. The selected compositions were designed to evaluate the effect of gradual Fe_2O_3 addition (0–1.5 mol%) on the shielding efficiency and radiation stability of bismuth borate glasses. This concentration range preserves the amorphous nature of the glass while enabling systematic tuning of density and photon interaction mechanisms. About 40 g glass batches were prepared according to each glass composition in porcelain crucibles. **Table 1** provides a summary of the wt% for all compositions and densities of each sample.

Table 1. The concentration of elements (wt%) in all samples.

Sample	Density (g/cm^3)	B (wt%)	O (wt%)	Bi (wt%)	Mg (wt%)	Na (wt%)	Al (wt%)	Fe (wt%)
1	.889	.1754	.4822	.2422	.0423	.0266	.0313	0
2	.902	.1733	.4797	.2410	.0420	.0265	.0311	.0064
3	.918	.0608	.3633	.0852	.0149	.0094	.0110	.4554
4	.952	.1690	.4747	.2385	.0416	.0262	.0308	.0191

The chemical materials used for glass preparation include H_3BO_3, Bi_2O_3, $MgCO_3$, Na_2CO_3, Al_2O_3, and Fe_2O_3, all sourced from Sigma-Aldrich with a purity of 99.9%. The first sample served as a baseline, comprising oxides B_2O_3, Bi_2O_3, MgO, Na_2O, and Al_2O_3, while the other three samples contain the same oxides, supplemented with iron oxide (Fe_2O_3) in different concentrations, with the highest concentration in the fourth sample. The mole fraction of each oxide in each sample is presented in **Table 2**.

Table 2. The mole fraction of each oxide in all samples.

Sample/ Mole fraction (%)	F1	F2	F3	F4
B_2O_3	70.00	69.5	69.00	68.50
Bi_2O_3	5.00	5.00	5.00	5.00
MgO	15.0	15.00	15.00	15.00
Na_2O	5.00	5.00	5.00	5.00
Al_2O_3	5.00	5.00	5.00	5.00
Fe_2O_3	0.00	0.50	1.00	1.50

In a muffle furnace, four accurately weighed batches were melted at temperatures ranging from 980 to 990 °C for 3 hours, with careful stirring at intervals to ensure homogeneity. The molten glass was then cast into preheated stainless-steel molds and immediately transferred to a second muffle furnace for annealing at 450 °C. This step was crucial for stress relief and to eliminate thermal strain within the glasses. After approximately 1 hour, the annealing furnace was turned off, and the glasses were allowed to cool to room temperature at a controlled rate of 30 °C/h. The thickness of the prepared samples was 0.2 cm ±0.01. XRD pattern of the prepared samples made by authors [33] revealed completely amorphous bands, indicating the glassy nature of the prepared samples.

ESR measurements

Electron spin resonance (ESR) spectra were recorded using an EMX spectrometer (X-band) with a standard Bruker ER 4102 rectangular cavity (Germany). The operating parameters for the ESR spectrometer were as follows: microwave power of 0.796 mW, modulation amplitude of 5 Gauss, time constant of 81.92 ms, and conversion time of 20.48 ms. Powdered samples were placed in ESR tubes and measured under the aforementioned parameters. All ESR measurements were conducted at laboratory temperature (25 ± 2 °C) during a single scan. A ^{60}Co gamma cell (2000 Ci) served as the gamma-ray source, delivering a dose rate of 0.686 kGy/h at 25 ± 5 °C.

Gamma-ray attenuation measurements

The gamma-ray count rates for the four glass samples were measured using a high-resolution planar germanium detector (Canberra, model GL0515R) with a 540 mm² active area, 1.5 cm height, and 540 eV (FWHM) resolution at 122 keV to assess their suitability as radiation shields. The measurements were conducted with two radioactive sources, ^{137}Cs and ^{60}Co, at three distinct energies: 0.662 MeV, 1.173 MeV, and 1.333 MeV. Energy calibration of the HPGe detector was performed before to sample measurement to ensure accuracy.

Theoretical calculations

The theoretical calculations were done using XCOM through the official website, and Phy-X/PSD calculations were done through the software by entering the compositions at energies range from 0.015 MeV to 15 MeV. Monte Carlo simulations were performed using the MCNP5 code to validate the experimental gamma-ray attenuation measurements. The simulation geometry is presented in **Figure 1**, which consists of a monoenergetic point gamma-ray source, the glass sample modeled as a cylindrical slab with thickness matching the experimental samples (0.2 cm), and an ideal detector placed directly behind the sample along the photon beam axis. The source-to-sample and sample-to-detector distances were fixed to minimize scattering effects and ensure narrow-beam geometry conditions.

The glass compositions were defined using experimentally measured densities and elemental weight fractions. Photon histories exceeding 10^8 were tracked to ensure statistically reliable results, and the F4 tally was employed to calculate the transmitted photon flux. Mass attenuation coefficients were then derived from the simulated intensity ratios using Beer–Lambert's law.

In this work, the validity of the MCNP5 simulation results was confirmed through direct cross-comparison with both theoretical and experimental data. The simulated mass attenuation coefficients were benchmarked against XCOM and Phy-X/PSD calculations over the same photon energy range, as well as against experimentally measured values obtained using the HPGe detector at 0.662, 1.173, and 1.333 MeV. The relative deviations between MCNP5, XCOM, and experimental MAC values were found to be in agreement,

which lies within the combined experimental and statistical uncertainties. This close agreement demonstrates the reliability of the adopted simulation geometry, material definitions, and photon transport parameters.

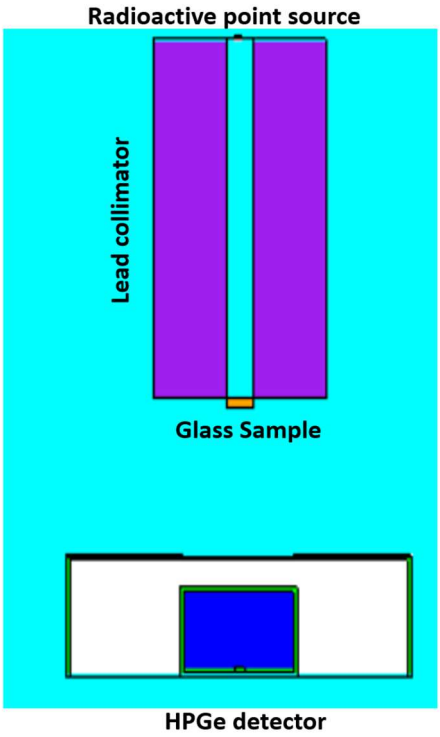

Figure 1. Schematic diagram of the MCNP5 simulation geometry used for gamma-ray attenuation calculations.

Results and discussions

ESR Analysis

The ESR spectra of the unirradiated samples exhibit broad resonance lines characteristic of transition-metal centers and intrinsic structural defects. The observed g ≈ 2.06 signal suggests the presence of Bi^{3+} ions in this coordination as well as Fe^{3+} species contributing to the paramagnetic signature. **Figure 2** presents the ESR spectra of the prepared Fe-lead bismuth glasses before irradiation, highlighting the intrinsic paramagnetic properties of the samples.

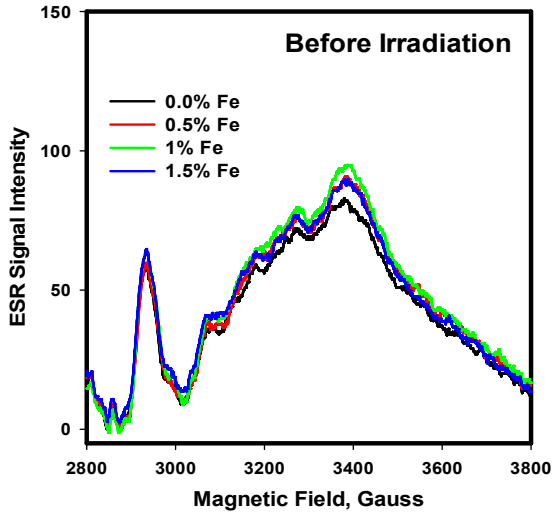

Figure 2. ESR spectra of the prepared Fe-lead bismuth glasses before irradiation

Following gamma irradiation up to 60 kGy, no appreciable changes are observed in peak position, line width, or intensity for any sample. **Figure 3** illustrates the ESR spectra of the same glasses after exposure to a gamma radiation dose of 60 kGy.

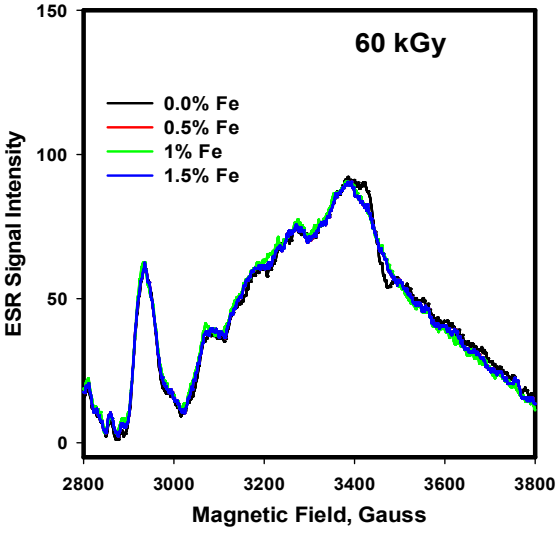

Figure 3. ESR spectra of the prepared Fe-bismuth borate glasses after gamma irradiation with 60 kGy

The strength and characteristics of ESR signals mainly depend on the concentration of irradiation-induced free radicals, such as trapped positive holes or electrons localized at various positions within the glass network. The previous Figures 2 and 3 show the ESR spectra

of both undoped and Fe-doped bismuth borate glasses before and after exposure to 60 kGy of gamma radiation. The spectral patterns for all four glass compositions were almost unchanged after irradiation, and no additional sharp ESR features were observed. This behavior implies that irradiation did not generate detectable free radicals and that significant bond rupture is unlikely to have occurred.

The exceptional stability under irradiation is attributed to the strongly interconnected bismuth borate network, primarily composed of trigonal BO_3 units and tetrahedral BO_4 groups. These structural units, together with the presence of heavy Bi^{3+} ions (high atomic number), enhance the ability to absorb gamma photons without causing noticeable modifications in the glass structure or disrupting bond connectivity. Furthermore, the inclusion of Fe^{3+} ions contributes to this stability; as transition-metal ions with variable oxidation states, they can donate or accept electrons, thereby compensating for or neutralizing defect color centers that may form under irradiation [19].

The high polarizability of Bi^{3+} ions helps hinder photon penetration, while the Fe^{2+}/Fe^{3+} redox pair increases the ability of the glass to absorb and eliminate irradiation-induced defects. In addition, the presence of condensed AlO_4 units enhances the rigidity and compactness of the glass network. The consistent ESR response and stability of the Fe-doped bismuth borate glasses under ionizing radiation highlight their strong potential as durable materials for radiation-shielding applications [34, 35].

Mass Attenuation Coefficient (MAC)

The (MAC, μ/ρ) of the base bismuth borate glass sample F1 was evaluated over a wide photon energy range from 0.015 to 15 MeV using the XCOM database and the Phy-X/PSD program. The obtained results are presented in **Figure 4.**

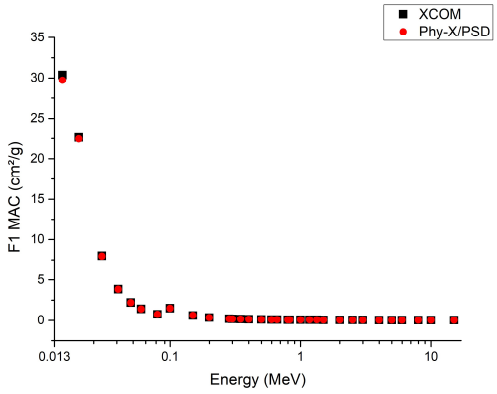

Figure 4. MAC results for the F1 sample by XCOM and Phy-X/PSD at different energies.

At low photon energies (0.015–0.06 MeV), the MAC values of sample F1 exhibit very high magnitudes, reaching 30.360 cm^2/g at 0.015 MeV according to XCOM and 29.701 cm^2/g using Phy-X/PSD. This strong attenuation capability in the low-energy region is primarily attributed to the dominance of the photoelectric absorption process, which is highly sensitive to photon energy and atomic number. The presence of Bi_2O_3 in the glass composition plays a crucial role in enhancing gamma-ray absorption in this region due to the high atomic number of bismuth.

As the photon energy increases from 0.02 to 0.3 MeV, a sharp decline in MAC values is observed. For example, the MAC decreases

from approximately 22.6 and 22.4 cm²/g at 0.02 MeV to about 0.179–0.180 cm²/g at 0.30 MeV in XCOM and Phy-X/PSD respectively. This rapid reduction is associated with the decreasing probability of photoelectric interactions and the gradual transition toward Compton scattering as the predominant photon interaction mechanism.

In the intermediate energy region (0.3–1.5 MeV), which includes the characteristic gamma-ray energies of ^{137}Cs (0.662 MeV) and ^{60}Co (1.173 and 1.333 MeV), the MAC values decrease more gradually. At 0.662 MeV, the MAC values are 0.084 and 0.085 cm²/g for XCOM and Phy-X/PSD, respectively, while at 1.333 MeV, both methods yield an identical value of 0.055 cm²/g. This behavior confirms that Compton scattering, which depends mainly on electron density rather than atomic number, dominates photon interactions in this energy range.

At higher photon energies above 2 MeV, the MAC values continue to decrease slowly and eventually reach a nearly constant value of about 0.028 cm²/g beyond 8 MeV. This plateau behavior is characteristic of the pair production region, where the attenuation coefficient becomes weakly dependent on photon energy and material composition.

A close comparison between XCOM and Phy-X/PSD results reveals an excellent consistency across the entire energy range, with only negligible differences observed at very low energies. This strong agreement validates the reliability of the computational methods used and confirms the accuracy of the MAC data for the investigated glass system. All the previous findings demonstrate that the base glass sample F1 has an effective gamma-ray attenuation performance, particularly at low and intermediate photon energies, mainly due to the incorporation of Bi_2O_3. These results establish F1 as a suitable reference material for assessing the impact of Fe_2O_3 addition on the radiation shielding efficiency of the investigated glass system.

A comparative analysis was conducted between the experimentally measured MAC of the base glass sample F1 and the corresponding theoretical values obtained using the XCOM database and MCNP5 simulations at photon energies of 0.6617, 1.173, and 1.333 MeV. The comparison results are illustrated in **Figure 5**.

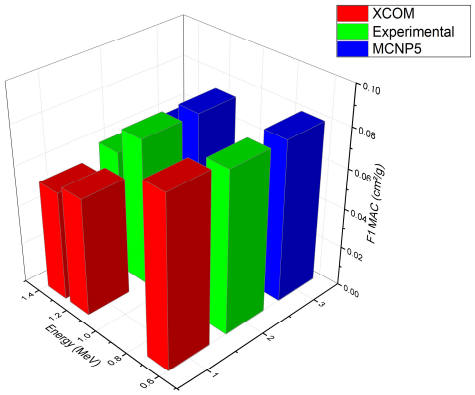

Figure 5. Comparison of experimental MAC results for the F1 sample with XCOM and MCNP5.

Figure 5 shows that, at 0.6617 MeV, the experimental MAC value (0.080613 cm²/g) is slightly lower than the XCOM result (0.085 cm²/g) but shows excellent agreement with the MCNP5 value (0.080627 cm²/g), with a negligible relative deviation. This close correspondence indicates the high accuracy of the Monte Carlo simulation in reproducing

experimental photon–matter interactions at this energy.

For higher photon energies of 1.173 and 1.333 MeV, the experimental MAC values (0.073618 and 0.060908 cm²/g, respectively) are higher than those predicted by XCOM (0.059 and 0.055 cm²/g). However, they remain in very good agreement with the MCNP5 results, where the deviations between experimental and simulated values are minimal. This behavior can be attributed to the ability of MCNP5 to account for detailed material composition, photon transport, and experimental geometry, whereas XCOM provides idealized cross-section data based on elemental mass fractions.

The observed discrepancies between the experimental and XCOM values, particularly at higher energies, are within acceptable limits. The strong agreement between experimental measurements and MCNP5 simulations confirms the reliability of the experimental setup and validates the use of Monte Carlo methods for accurately predicting gamma-ray attenuation behavior in bismuth borate glass systems.

The (MAC, μ/ρ) of the Fe_2O_3-doped bismuth borate glass samples F2, F3, and F4 were evaluated over the photon energy range of 0.015–15 MeV using the XCOM database and the Phy-X/PSD program. The calculated results are illustrated in **Figures 6, 7,** and **8** respectively, and demonstrate an excellent agreement between the two computational approaches across the entire investigated energy spectrum.

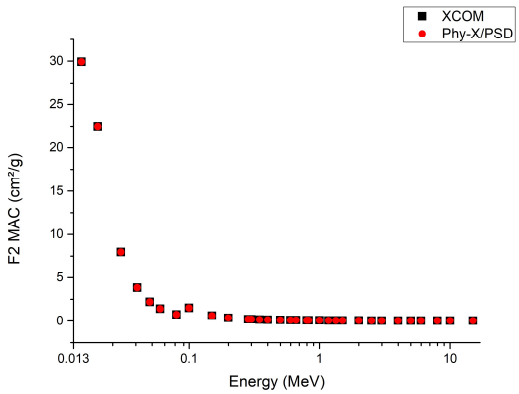

Figure 6. MAC results for the F2 sample by XCOM and Phy-X/PSD at different energies.

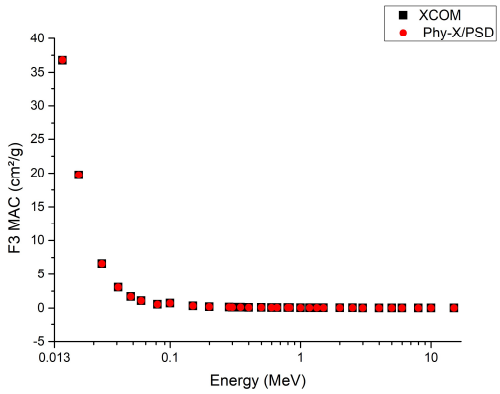

Figure 7. MAC results for the F3 sample by XCOM and Phy-X/PSD at different energies.

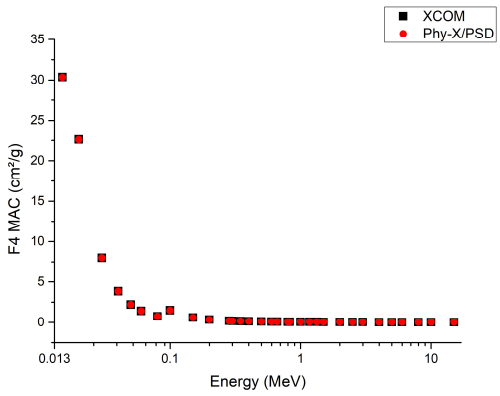

Figure 8. MAC results for the F4 sample by XCOM and Phy-X/PSD at different energies.

For all doped samples, the MAC values exhibit a strong energy dependence, characterized by very high attenuation at low photon energies followed by a continuous decrease with increasing energy. In the low-

energy region ($E \leq 0.06$ MeV), the MAC values using Phy-X/PSD reach their maximum, with F3 showing the highest value of 36.798 cm^2/g at 0.015 MeV, compared to 29.914 cm^2/g for F2 and 30.333 cm^2/g for F4. This behavior is attributed to the dominance of the photoelectric absorption process, which is highly sensitive to both photon energy and effective atomic number. The observed enhancement in F3 indicates that the incorporation of Fe_2O_3 alters the glass network and effective atomic number, leading to noticeable changes in photon interaction probability at very low energies.

As the photon energy increases from 0.02 to approximately 0.3 MeV, a sharp reduction in MAC values is observed for all doped samples. For instance, the MAC of F2 decreases from about 22.48 cm^2/g at 0.02 MeV to 0.18 cm^2/g at 0.30 MeV, while F3 decreases from 19.75 to 0.134 cm^2/g over the same energy interval. This rapid decline reflects the diminishing contribution of photoelectric absorption and the gradual transition toward Compton scattering as the dominant interaction mechanism.

In the intermediate energy range (0.3–1.5 MeV), which includes the characteristic gamma energies of ^{137}Cs and ^{60}Co, the MAC values decrease more gradually and become closer for all samples. At 0.662 MeV, the MAC values using XCOM are 0.085, 0.078, and 0.084 cm^2/g for F2, F3, and F4, respectively. Similarly, at 1.333 MeV, the corresponding values are 0.055, 0.053, and 0.055 cm^2/g. This convergence confirms the Compton scattering.

At higher photon energies ($E \geq 2$ MeV), the MAC values for F2, F3, and F4 exhibit a slight decrease and eventually approach nearly constant values of approximately 0.028 cm^2/g beyond 8 MeV. This plateau-like behavior is characteristic of the pair production region, where the attenuation process becomes weakly dependent on energy and minor compositional variations.

A close comparison between XCOM and Phy-X/PSD results reveals an almost acceptable overlap for all doped samples, with negligible deviations across the studied energy range. This excellent agreement confirms the reliability of both computational tools and validates their applicability for predicting gamma-ray attenuation properties of Fe-doped bismuth borate glass systems.

A comparative evaluation was performed between the experimentally measured mass attenuation coefficients (MAC) of the Fe_2O_3-doped glass samples F2, F3, and F4 and the corresponding theoretical values obtained from XCOM and MCNP5 at photon energies of 0.6617, 1.173, and 1.333 MeV. These comparisons are illustrated in **Figures 9, 10,** and **11**.

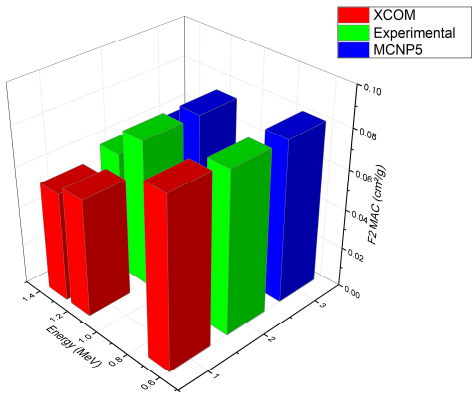

Figure 9. Comparison of experimental MAC results for the F2 sample with XCOM and MCNP5.

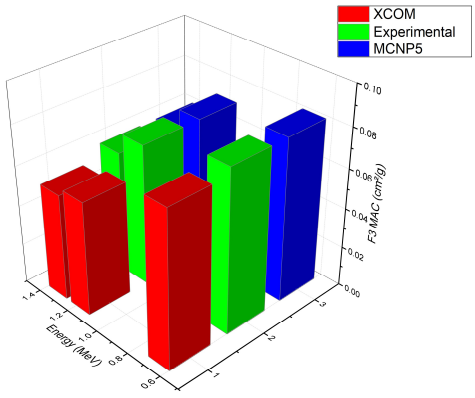

Figure 10. Comparison of experimental MAC results for the F3 sample with XCOM and MCNP5.

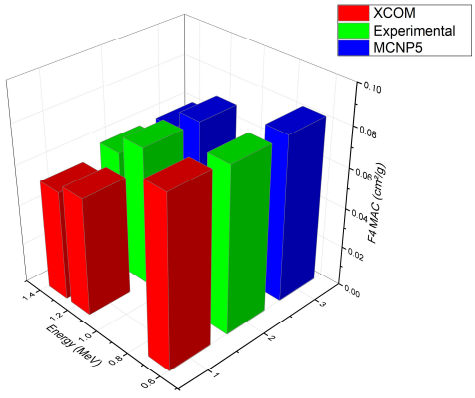

Figure 11. Comparison of experimental MAC results for the F4 sample with XCOM and MCNP5.

For sample F2, the experimental MAC values at 0.6617, 1.173, and 1.333 MeV (0.081102, 0.073288, and 0.060503 cm²/g, respectively) are slightly lower than the XCOM predictions at 0.6617 MeV but higher at the ^{60}Co energies. In contrast, a good agreement is observed between the experimental measurements and MCNP5 results, with only negligible deviations across all investigated energies.

A similar trend is observed for sample F3, where the experimental MAC values are consistently closer to the MCNP5 results than to those obtained from XCOM. At 0.6617 MeV, the experimental MAC (0.081777 cm²/g) slightly exceeds the XCOM value (0.078 cm²/g), while at higher energies (1.173 and 1.333 MeV), the experimental results remain notably higher than the XCOM predictions. The close overlap between experimental and MCNP5 values demonstrates the robustness of the simulation in accounting for compositional effects introduced by Fe_2O_3 doping.

For sample F4, the experimental MAC values (0.082404, 0.069139, and 0.060255 cm²/g at 0.6617, 1.173, and 1.333 MeV, respectively) again show a consistency with MCNP5 calculations, whereas modest discrepancies are observed when compared to XCOM data, particularly at the ^{60}Co energies. These deviations can be attributed to the idealized nature of XCOM calculations.

Linear Attenuation Coefficient (LAC)

The (LAC, μ) of the investigated bismuth borate glass samples (F1–F4) was evaluated over the photon energy range of 0.015–15 MeV using the corresponding mass attenuation coefficients and the experimentally measured densities. The obtained LAC values for all samples are illustrated in **Figure 12**.

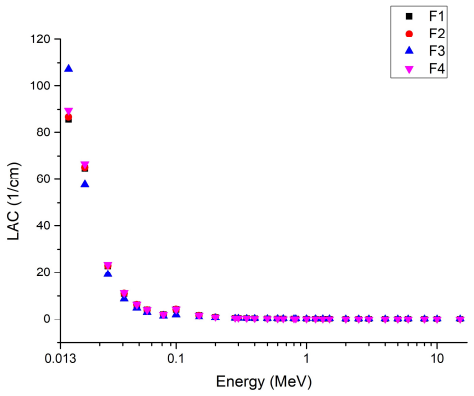

Figure 12. LAC results for all samples by Phy-X/PSD.

In the low-energy region (E ≤ 0.06 MeV), the LAC values are markedly high for all samples, reaching maximum values of 85.806, 86.810, 107.378, and 89.542 cm^{-1} for F1, F2, F3, and F4 at 0.015 MeV, respectively. This behavior is consistent with the MAC profiles and is attributed to the dominance of the photoelectric absorption process. Among the investigated samples, F3 exhibits the highest LAC values in this region, reflecting its enhanced photon absorption capability due to compositional modifications introduced by Fe_2O_3 doping and its associated density variation.

As photon energy increases from 0.02 to approximately 0.3 MeV, a sharp reduction in LAC values is observed for all samples. For example, the LAC of F1 decreases from 64.805 cm^{-1} at 0.02 MeV to 0.521 cm^{-1} at 0.30 MeV, while a similar trend is noted for the other compositions. This rapid decline mirrors the behavior observed in the MAC results and indicates the decreasing contribution of photoelectric absorption with increasing energy.

In the intermediate energy region (0.3–1.5 MeV), the LAC values decrease more gradually and the differences between samples become less pronounced. At 0.6617 MeV, the LAC values using Phy-X/PSD range from 0.228 cm^{-1} for F3 to 0.249 cm^{-1} for F4, while at 1.333 MeV they lie within a narrow range of 0.156–0.161 cm^{-1}. This convergence is in good agreement with the MAC behavior in the same energy region, confirming that Compton scattering dominates photon–matter interactions.

At higher photon energies (E ≥ 2 MeV), the LAC values exhibit a slight decrease and eventually approach nearly constant values above 8 MeV. For instance, at 10 MeV, the LAC values stabilize around 0.080–0.082 cm^{-1} for all samples. This plateau behavior is characteristic of the pair production region and closely follows the trend observed in the MAC profiles, indicating weak sensitivity to both energy and compositional variations at high energies.

Effective Atomic Number (Z_eff)

The effective atomic number is a key parameter governing photon–matter interaction processes and provides critical insight into the gamma-ray attenuation performance of shielding materials. The calculated Z_eff values for the investigated bismuth borate glass samples F1–F4 over the photon energy range of 0.015–15 MeV are presented in **Figure 13**.

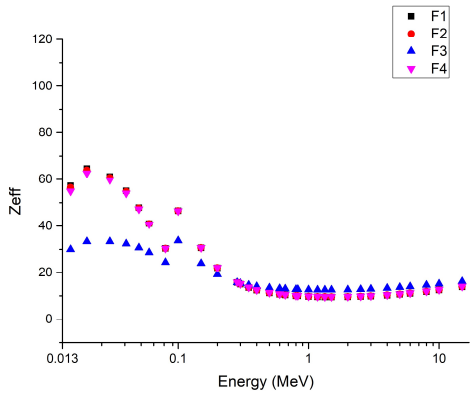

Figure 13. Zeff results for all samples by Phy-X/PSD.

At low photon energies (E ≤ 0.1 MeV), Z_eff exhibits pronounced energy dependence for all samples, with relatively high values resulting from the dominance of the photoelectric absorption mechanism. In this region, samples F1, F2, and F4 display comparable Z_eff values, reaching maxima of 57.24, 56.42, and 54.90 at 0.015 MeV, respectively. In contrast, sample F3 shows significantly lower Z_eff values (30), indicating a reduced contribution of high-Z constituents to photoelectric interactions in this specific composition. This behavior reflects the sensitivity of Z_eff to both elemental composition and photon energy, particularly in the photoelectric region where the interaction cross section strongly depends on atomic number.

With increasing photon energy from 0.1 to approximately 0.3 MeV, Z_eff decreases sharply for all samples, corresponding to the diminishing contribution of photoelectric absorption and the gradual transition to Compton scattering dominance. Around 0.284–0.300 MeV, the Z_eff values for all samples converge to a narrow range (average ≈15–16), indicating that compositional differences have a reduced influence on photon interactions in this energy region.

In the intermediate energy range (0.3–1.5 MeV), which includes the characteristic energies of ^{137}Cs and ^{60}Co, Z_eff values remain relatively stable and exhibit weak energy dependence. For samples F1, F2, and F4, Z_eff lies in the range of 9.5–10.5, while sample F3 consistently shows higher values (~12.6–13.0). This behavior is consistent with Compton scattering dominance, where Z_eff primarily reflects electron density rather than absolute atomic number. The elevated Z_eff values of F3 in this region suggest a higher effective electron density, which contributes positively to gamma-ray attenuation at intermediate energies.

At higher photon energies (E ≥ 2 MeV), Z_eff gradually increases for all samples, reaching maximum values at 15 MeV. This increase is attributed to the growing contribution of pair production, whose interaction probability scales with atomic number. At 15 MeV, Z_eff reaches 13.85, 13.91, 16.19, and 14.04 for F1, F2, F3, and F4, respectively. Among all samples, F3 maintains the highest Z_eff throughout the high-energy region, indicating its superior potential for gamma-ray attenuation at elevated photon energies. These findings are in good agreement with the trends observed in the MAC and LAC results and confirm that compositional tuning through Fe_2O_3 incorporation can significantly influence the photon interaction mechanisms

and shielding efficiency of bismuth borate glass systems.

Half-Value Layer (HVL) and Mean Free Path (MFP)

The half-value layer (HVL) and mean free path (MFP) are practical shielding parameters that directly quantify the thickness required to attenuate incident gamma radiation and the average distance traveled by photons within a material before interaction, respectively. Both parameters were derived from the calculated linear attenuation coefficients for the investigated glass samples F1–F4 over the photon energy range of 0.015–15 MeV. The corresponding values are illustrated in Figures 14 and 15.

Half-Value Layer (HVL)

Figure 14 shows the HVL values of all samples exhibit a strong dependence on photon energy, increasing monotonically with energy. At low photon energies (E ≤ 0.06 MeV), extremely small HVL values are observed, indicating good shielding efficiency. For example, at 0.015 MeV, the HVL values are 0.008, 0.008, 0.006, and 0.008 cm for F1, F2, F3, and F4, respectively. This behavior is consistent with the dominance of photoelectric absorption, as previously confirmed by the MAC and Z_eff results.

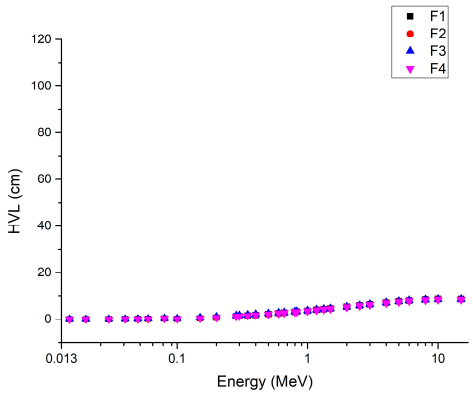

Figure 14. HVL results for all samples by Phy-X/PSD.

As photon energy increases, HVL values rise rapidly due to the reduction in interaction probability. In the intermediate energy region (0.3–1.5 MeV), HVL values increase gradually and show moderate compositional dependence. At 0.6617 MeV, the HVL values range from 2.781 cm (F4) to 3.040 cm (F3), while at 1.333 MeV they vary between 4.299 and 4.445 cm. The slightly higher HVL values observed for sample F3 indicate reduced attenuation efficiency, which is consistent with its comparatively lower LAC and MAC values in this energy range.

At higher photon energies (E ≥ 2 MeV), the HVL values continue to increase and eventually approach near-constant values above 8 MeV. At 10 MeV, the HVL values lie between 8.48 and 8.69 cm for all samples, reflecting the dominance of pair production and the reduced sensitivity of attenuation to compositional variations. Among the investigated glasses, samples F4 and F1 consistently exhibit lower HVL values across most energies, indicating superior shielding performance.

Mean Free Path (MFP)

The MFP results in **Figure 15** show trends similar to those observed for HVL, as both parameters are inversely proportional to the linear attenuation coefficient. At low photon energies, very small MFP values are recorded, confirming frequent photon interactions within short distances. At 0.015 MeV, the MFP values are 0.012, 0.012, 0.009, and 0.011 cm for F1–F4, respectively, with sample F3 again showing the shortest photon travel distance due to its higher interaction probability in this region.

With increasing photon energy, MFP values increase significantly. In the intermediate energy region, MFP values range from approximately 4.01 to 4.39 cm at 0.6617 MeV and from 6.20 to 6.41 cm at 1.333 MeV. Sample F3 consistently exhibits the highest MFP values, while F4 and F1 show lower values, indicating improved shielding effectiveness. At high energies ($E \geq 8$ MeV), the MFP values approach saturation, reaching approximately 12.2–12.5 cm at 10–15 MeV for all samples.

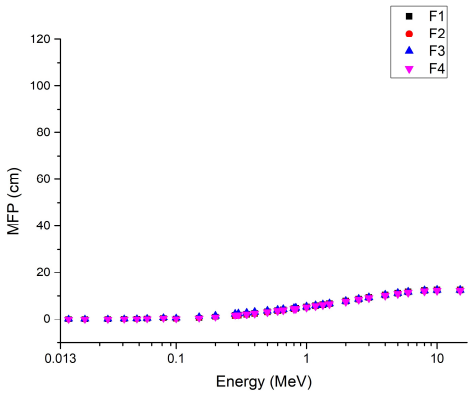

Figure 15. MFP results for all samples by Phy-X/PSD.

Conclusion

Fe_2O_3-doped bismuth borate glasses were successfully synthesized and evaluated for their gamma-ray attenuation efficiency and structural stability. Experimental MAC values obtained using HPGe detector showed good agreement with XCOM, MCNP5, and Phy-X/PSD predictions, confirming the validity of the computational approaches and the consistency of the measurements. The gamma-ray attenuation behavior of the investigated glasses shows a pronounced energy dependence controlled by the dominant photon interaction mechanisms. High attenuation at low energies is governed by photoelectric absorption, enhanced by the presence of high-Z constituents such as Bi_2O_3, while Compton scattering dominates the intermediate energy region, leading to convergent attenuation parameters with minimal compositional influence. At higher photon energies, the stabilization of MAC and LAC values and the increase in effective atomic number indicate the growing contribution of pair production. ESR analyses revealed that all glasses retained exceptional structural integrity after irradiation up to 60 kGy, with no measurable changes in g-values, linewidths, or signal intensity. This radiation resilience is attributed to the combined stabilizing effects of Bi^{3+} ions and the Fe^{2+}/Fe^{3+} redox pair, which effectively suppress the generation and trapping of irradiation-induced defects. Finally, Fe_2O_3 addition slightly alters low-energy attenuation behavior without degrading shielding efficiency at medium and high energies. The

corresponding HVL and MFP results confirm effective gamma-ray attenuation with relatively small material thicknesses, demonstrating that Fe-doped bismuth borate glasses offer tunable shielding performance while maintaining practical efficiency with potential for use in medical imaging, industrial radiography, and nuclear radiation-protection technologies. Future work may explore long-term durability and integration into real-world shielding systems.

Author contributions

All authors contributed to the study conception and design. Data collection, Methodology, analysis. Supervision was performed by [S. E. Shaban[1*]]. The first draft of the manuscript was written by [S.E. Shaban[1*]]. [E.M. Abou Hussein[2]] prepared material and ESR spectra. [M. A. Samei[1]] participated in finalizing gamma Measurements. [S. E. Shaban[1*]] used XCOM and Phy-X/PSD to assess the shielding parameters. All authors commented on previous versions of the manuscript. All authors read and approved the final manuscript.

Declaration of generative AI and AI-assisted technologies in the writing process

During the preparation of this work the authors used AI tools and Grammarly in order to enhance language in the final form. After using these tools, the authors reviewed and edited the content as needed and take full responsibility for the content of the publication.

References

[1] Aydin H, Süsoy Doğan G, Tekin H, Şen Baykal D, İltuş Y. Examining the Neutron and Gamma Attenuation Characteristics of Various Amorphous Structures with Bioactive Properties. International Journal of Computational and Experimental Science and Engineering 2025;11(3).

[2] Soriano-Romero O, Lozada-Morales R, Meza-Rocha A, Carmona-Téllez S, Caldiño U, Flores-Desirena B, Palomino-Merino R. Cold bluish white and blue emissions in Cu+-doped zinc phosphate glasses. Journal of Luminescence 2020;217:116791.

[3] Jiménez J. Spectroscopic inquiry of CuO-doped borate glasses in the 50B2O3-25Li2O-25BaO ternary. Spectrochimica Acta Part A: Molecular and Biomolecular Spectroscopy 2021;262:120113.

[4] Demet Sariyer, Elif Yıldırım. A Hybrid Monte Carlo–Machine Learning Framework for High-Energy Neutron Shielding Using Boron-Enhanced Concrete. International Journal of Computational and Experimental Science and Engineering 2026;12(1):447–461.

[5] Sağlam F, Cetin B. Investigation of Gamma Shielding Properties of Some Industrial Materials. International Journal of Computational and Experimental Science and Engineering 2025;11(2).

[6] Seher Polat, Mucize Sarıhan, Roya Boudaghi Malidarreh3, Sabiha Anas Boussaa, Nurdan Karpuz, Nuray Kutu. ANN Prediction of Linear Attenuation Coefficients for 40MgO–30B2O3–30SiO2 System. International Journal of Applied Sciences and Radiation Research 2026;3(1).

[7] Sibel Özavci, Betül Çetin. Experimental Investigation of Radiation Shielding Effect in Different Doped Slag Concrete. International Journal of Sustainable Science and Technology 2025;1(1).

[8] Abou Hussein E, Shaban S, Makhlouf S. Unveiling the effect of CeO2 addition on optical, physical and radiation shielding efficiency in binary lead borate glasses. Radiation Physics and Chemistry 2025;235:112762.

[9] Emikönel S, İskender A. Radiation Shielding Properties of B2O3-Bi2O3 Glass. International Journal of

Computational and Experimental Science and Engineering 2025;11(2).

[10] Demet Sarıyer. FLUKA Monte Carlo Assessment of Fe_2B-Based Shielding Materials for Secondary Neutrons in a 1000 MeV Proton Accelerator. International Journal of Computational and Experimental Science and Engineering 2025;11(4).

[11] Morad Kh. Hamad . Synergistic Evaluation of Ionizing Radiation Shielding in Novel Lead-Free Alloys Using Geant4 MC toolkit. International Journal of Applied Sciences and Radiation Research 2025;2(1).

[12] Günoğlu K, Akkurt I. Gamma-ray attenuation properties carbide compounds (WC, Mo2C, TiC, SiC, B4C) using Phy-X/PSD software. International Journal of Applied Sciences and Radiation Research 2023;1(1):1-8.

[13] Calas G, Capobianco N, Galoisy L. Spectroscopic properties of alkali borate glasses containing Cu2+. Journal of Non-Crystalline Solids 2022;591:121711.

[14] Lv T, Xu X, Zhou D, Qiu J. Influence of Cu+ cations on photoluminescence properties of Tb3+ in Cu+–Na+ ion-exchanged sodium-borosilicate glasses. Journal of Non-Crystalline Solids 2015;409:14-19.

[15] Duffy J. Redox equilibria in glass. Journal of Non-Crystalline Solids 1996;196:45-50.

[16] Jiménez J. What is the origin of concentration quenching of Cu+ luminescence in glass?. Physica B: Condensed Matter 2016;498:92-97.

[17] Alharshan G, Shaaban S, Elsafi M, Elsad R, Said S, Mahmoud A, Bahei El-Deen A, Mimouni A. The impact of bismuth doping on the mechanical, optical, and radiation-shielding properties of borosilicate glass systems. Egyptian Journal of Chemistry 2025;0(0):0-0.

[18] Saeed A, Abo Zeed M, ElShazly R, El Esh E, El-Mallah H. Evaluation of Gamma-Rays Attenuation Parameters for Novel Lead-Borate Glass System. Egyptian Journal of Chemistry 2023;0(0):0-0.

[19] Gasser R, Yassin O, Salem S. Structural Characterization and Gamma-Ray Shielding- Parameters of Some Phosphate Glasses Containing By-Pass Cement Dust and Barium Oxide. Egyptian Journal of Chemistry 2021;0(0):0-0.

[20] Al-Buriahi M, Alsaiari N, Baskin M, Olarinoye I. Recent progress in the radiation shielding performance of common glass systems: The roles of different class of modifiers. Journal of Radiation Research and Applied Sciences 2025;18(1):101264.

[21] Zhang J, Moine B, Pedrini C, Parent C, Flem G. Optical spectroscopy of monovalent copper-doped borate glasses. Journal of Physics and Chemistry of Solids 1990;51(8):933-939.

[22] Verwey J, Coronado J, Blasse G. The luminescence of Cu(I) in strontium tetraborate. Journal of Solid State Chemistry 1991;92(2):531-536.

[23] Mott NF, Davis EA. Electronic Processes in Non-Crystalline Materials Clarendon-Press, Oxford 1971 437 Seiten. £ 7,50. Kristall und Technik 1972;7(4).

[24] Malacara D. Color Vision and Colorimetry: Theory and Applications, Second Edition 2011.

[25] Mortimer R, Varley T. Quantification of colour stimuli through the calculation of CIE chromaticity coordinates and luminance data for application to in situ colorimetry studies of electrochromic materials. Displays 2011;32(1):35-44.

[26] Sigel Jr, Ginther RG. The effect of iron on the ultraviolet absorption of high purity soda-silica glass, Glass Technol. 1968;9:66.

[27] Cook L, Mader K. Ultraviolet Transmission Characteristics of a Fluorophosphate Laser Glass. Journal of the American Ceramic Society 1982;65(12):597-601.

[28] Alotaibi B, Alhuzaymi T, Alotiby M, Makhlouf S, Shaaban K, Abdel Wahab E. Optical structural and radiation shielding efficiency of vanadium-doped LZBS glass. Optik 2024;301:171689.

[29] Betul Cetin, Arzu Poyraz, Melek Gul. Examination of the radiation absorption parameters of CuO coatings prepared at different ratios. International Journal of Sustainable Science and Technology 2025;4(1).

[30] Waheed F, Iskender Akkurt. The Experimental Enhancing of the Radiation Shield Properties of Some Produced Compounds. International Journal of Applied Sciences and Radiation Research 2025;2(1).

[31] Abuş F, Gürçalar A, Günay O, Tunçman D, Kesmezacar F, Demir M. Quantification of Lens Radiation Exposure in Scopy Imaging: A Dose Level Analysis. International Journal of Applied Sciences and Radiation Research 2024;1(1).

[32] Soyal H, Sarıhan M. The Place, Importance and Development Approaches of Radiation Safety and Protection Education in Associate Degree Health Programs. International Journal of Sustainable Science and Technology 2025;1(1).

[33] Abou Hussein E, Barakat M. Structural, physical and ultrasonic studies on bismuth borate glasses modified with Fe2O3 as promising radiation shielding materials. Materials Chemistry and Physics 2022;290:126606.

[34] Abou Hussein E, Shaban S, Rammah Y, Misbah M, Marzouk M. Newly developed CeO2 and Gd2O3-reinforced borosilicate glasses from municipal waste ash and their optical, structural, and gamma-ray shielding properties. Scientific Reports 2024;14(1):13673.

[35] Abou Hussein E, Madbouly A. Fabrication and characterization of different PbO borate glass systems as radiation-shielding containers. Scientific Reports 2024;14(1):2638.